Design and Simulation of A MEMS Based Horseshoe Shaped Low Current Lorentz Deformable Mirror (LCL-DM).

Byoungyoul Park[1], Tao Chen[1], Cyrus Shafai[1]
[1]Electrical and Computer Engineering, University of Manitoba, Winnipeg, Manitoba, Canada.
*Corresponding author: E3-473 EITC, University of Manitoba, Winnipeg, MB R3T 5V6 Canada, parkb3@myumanitoba.ca

Abstract: This paper presents the design and analysis of a novel horseshoe shaped MEMS actuator for adaptive optics. The actuation mechanism is Lorentz force enabling low current (below 10 mA) operation. The actuator combined with an overlying aluminum coated SU-8 soft polymer membrane for the mirror, together form the complete adaptive optics system to enable correction of wavefront distortion of optical aberrations. Simulations using COMSOL Multiphysics software detail actuator design, mirror motion, and inter-element crosstalk between actuators. Thermal effect by Joule heating, a major drawback of high current actuators, is simulated, and show the Lorentz actuator has less than 0.1 K temperature change.

Keywords: Lorentz Actuator, MEMS, SU-8, Epoxy, Adaptive Optics (AO), Deformable Mirror (DM)

1. Introduction

A deformable mirror (DM) is used to achieve wavefront control and correction of optical aberrations in many optical systems, such as, telescopes [1], retinal imaging systems [2], and optical communications [3]. Micro-electromechanical system (MEMS) fabrication technologies can be used to miniaturize actuator elements to decrease high power consumption, reduce space occupancy, and enable fabrication of large numbers of actuator elements together, increasing the reliability of the manufacturing process of compared to classical actuators.

MEMS actuators commonly use four main transduction mechanisms to enable motion displacement: electrostatic, piezoelectric, thermal, and magnetic [4]. Within these variety of actuators, MEMS based electrostatic actuators are more widely used due to their high compatibility with the microfabrication process, their low power consumption, simple structure, and fast response. A first example of electrostatic MEMS actuators used for deformable mirrors (DM) was demonstrated by M. Yelling in 1976 [5]. However, they commonly require a high operation voltage and show nonlinear behavior. By contrast, Lorentz force excited MEMS actuators offer many advantages. They have bi-directional motion, with no magnetic hysteresis effects, enabling them to push upwards as well as pull downwards. This enables the correction of surface flatness issues due to gravity-induced deformation on larger diameter mirror membranes. These advantages, combined with a simple actuator design, fast response, reasonable power consumption, make them ideal for a large stroke application [6,7].

2. Structural Design

The low current Lorentz force deformable mirror (LCL-DM) system is comprised of an underlying horseshoe shaped actuator attached to an overlying mirror. Design specifications for the DM were ± 5 µm deformation, aluminum metal reflective surface, and below 10% inter-element crosstalk over for adjacent mirror locations above each actuator.

The horseshoe Lorentz actuator is designed based on flexible supporting arms and a central thick and rigid crossbar above a permanent magnet (see Figure 1). In this design, the generated Lorentz force on the crossbar can be calculated by using equation (1), which relates the magnetic field ($\vec{B}$), current ($\vec{\imath}$), and wire length (l) of the conductor [8].

$$\vec{F} = \vec{B} \times \vec{\imath}l \qquad (1)$$

The actuator array (Figure 2) is fabricated on a silicon wafer using a bulk micromachining process to free a cavity below each actuator. Each actuator possesses a stiff crossbar (crystalline silicon or electroplated copper), a central pillar on the crossbar connecting it to the above membrane mirror, and spring arms connecting the crossbar to the substrate. The spring arms provide mechanically support the crossbar, electrical

current pathway, and heat transfer to the substrate. The crossbar is designed to be rigid to limit its own bending when it applies force to the above membrane. The important concerns for the horseshoe shaped actuator and DM design are:

- Thick crossbar and soft supporting arms
- Soft polymer membrane with appropriate resonant frequency
- Bulk and surface micromachining
- Thermo-mechanical stability

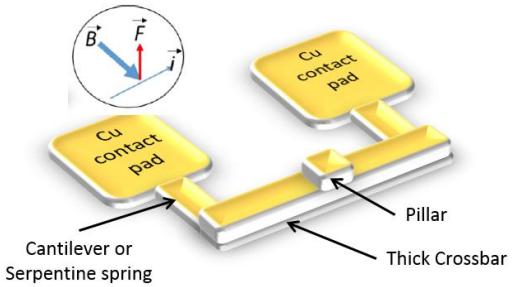

Figure 1. Illustration of Lorentz force actuator and force relationship (shown in the black circle).

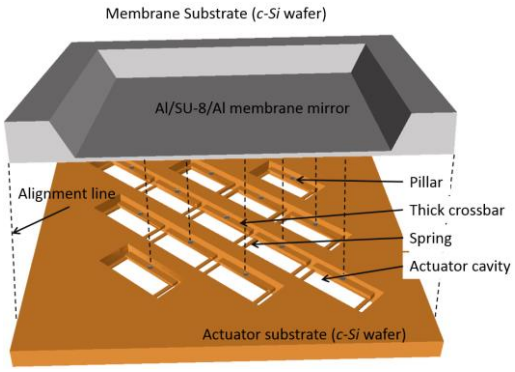

Figure 2. Illustration of a 3 x 3 array of Lorentz actuators below the DM structure.

Epoxy based negative tone photoresist SU-8 is selected as the materials for the mirror membrane, due to its low Young's modulus, smooth film surface, and compatibility with the semiconductor fabrication process. Several important material properties of the SU-8 are presented in Table 1. SU-8 was developed by IBM in 1989 [9] and is well established as a material for the fabrication of electroplating molds and general microstructures. Use of SU-8 for an electrostatic actuated DM was reported by C. Friese et, al., Robert Bosch GmbH, Germany [10].

Table 1. Thermal and mechanical property of SU-8

Material Properties	Value
Young's Modulus (Gpa)	2
Tensile Strength (Mpa)	60
Density (g/cm^3)	1.22
Thermal Conductivity (W/mK)	0.3
CTE (10^{-6} m/K)	50

3. Simulation

3.1. Deformable Mirror

A 3D model was constructed, with the horseshoe shaped Lorentz actuator below an overlying SU-8 membrane coated with a 150 nm aluminum reflective layer on both sides. The two sided aluminum coating is used for stress balancing. Two work planes are used, one for the actuator and central pillar, and the other for the continuous SU-8 membrane. The overall membrane thickness is fixed to 5.3 µm (0.15 µm Al / 5 µm SU-8 / 0.15 µm Al), and shows linear membrane deformation profiles with an applied force in the ± 5 µm displacement range. Various geometrical combinations are studied by parameterizing the entire structure. The overall simulation was broken down to three individual steps, in order to achieve accurate computation and reduce computation time.

STEP 1: Simulate the spring constant of a corner clamped SU-8 membrane over a 3x3 actuator array, with 2000 µm actuator pitch.
STEP 2: Simulate the spring constant of the spring supported crossbar.
STEP 3: Simulate the mechanical deformation behavior of the continuous SU-8 membrane spanning a 3x3 actuator array.

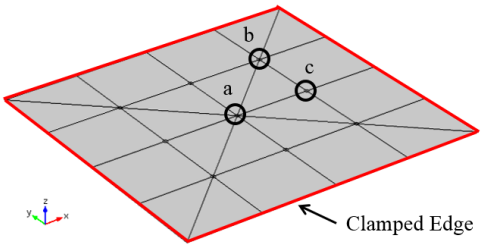

a. Force loading center.
b. 1st nearest pillar with pre-defined spring (clamped).
c. 2nd nearest pillar with pre-defined spring (clamped).

- Al mirror layer
- SU-8 ~ 5 μm thickness
- Al stress compensation and Bonding layer

Figure 3. Boundary conditions of the membrane and its vertical structure.

STEP 1 modeling:

Solid Mechanics in the Structural Mechanics module of COMSOL 4.3 was used for simulations. Figure 3 shows the boundary conditions of the corner clamped continuous membrane. This model uses the material properties listed in Appendix 1. The model consists of a 3 x 3 actuators array, beneath a continuous membrane clamped at the outer boundary. In the figure, the actuator-pillars connect to the membrane at the each inner node.

As a first simulation, the 1st and 2nd nearest actuator pillars are clamped to calculate a force for 5 µm in *z* directional membrane deformation. This result can give an approximate value for that required in STEP 3. Here, the clamping means that there is no translation or rotation permitted (x = 0, y = 0, and z = 0). The simulated spring constant of the membrane is 2.37 N/m. Figure 4 shows that the membrane achieves the desired near linear deformation profile below 6 µm deflection. Figure 5 shows the typical membrane deformation shape in which the deflection shows opposite direction in between the nearest neighbor actuator and the next in line, since the face-sheet pivots on the nearest neighbor pillar.

Using these results, we can simplify the model of the membrane for future simulations. Instead of simulating a multilayered Al/SU-8/Al membrane, we can simulate a single SU-8 membrane with additional thickness to account for the removed Al layers. From the above results, it was determined that an equivalent single SU-8 membrane would need to be 11 µm thick to provide the same deflection characteristics. This simpler structure is then used in subsequent simulations to reduce computation time.

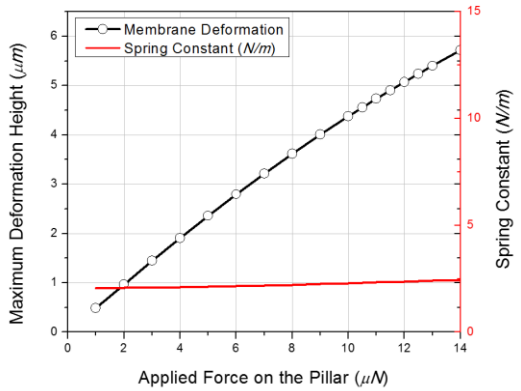

Figure 4. Double side aluminum coated SU-8 membrane deformation versus applied force, with determined membrane spring constant.

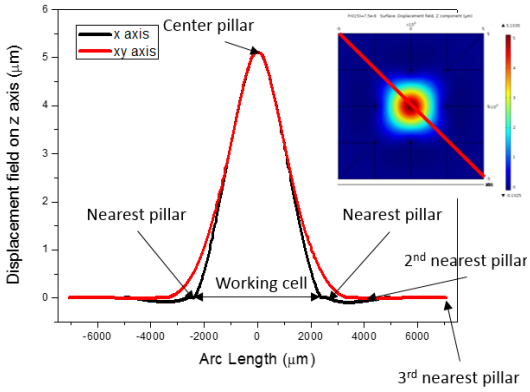

Figure 5. 5 µm membrane deformation profile in x and xy axis with 11.8 µN loading on the pillar, and with 1st and 2nd nearest pillar actuators fixed in place.

STEP 2 modeling:

With the membrane spring constant now known, the spring constant of the actuator is now determined. Initial simulations assumed a simple *c-Si* cantilever spring pushing against the membrane. 1000 µm long and 10 µm thick cantilevers with various widths are used for defining the spring constant of the actuator and the membrane crosstalk simultaneously. The simulation results shows excellent match with the calculation result by equation (2), as shown in Figure 6. In Figure 6, F is the applied force at the end of cantilever, t is the cantilever thickness, l is the cantilever length, w is the cantilever width, d is maximum cantilever deformation distance, and E is Young's modulus.

$$t = \sqrt[3]{\frac{4Fl^3}{Ewd}} \qquad (2)$$

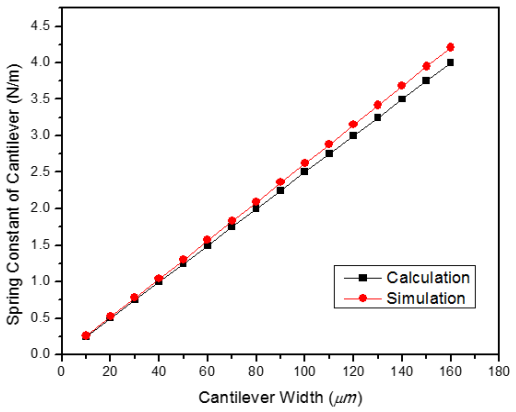

Figure 6. Cantilever spring constant with various width (red; simulation result, black; calculation result).

STPE 3 modelling:

The mechanical crosstalk of the LCL-DM can now be studied by combining steps 1 and 2. In Figure 3, cantilevers and pillar structures are shown constructed beneath the 1st and 2nd nearest actuator place. Other pillars and all membrane edges are clamped. To examine the spring rigidity and membrane deformation, the force is applied on the center pillar region (point of Figure 3), and studied for various widths of cantilevers. Simulation results are shown in Figure 7. A more rigid actuator requires more force to deform a membrane, but increases a resonant frequency of the DM. On the other hand, softer actuators reduce the operation power but gives higher mechanical crosstalk on the membrane.

From Figure 7, we can see that an actuator with a 1 N/m spring constant shows only 10 % crosstalk with an 11 μN force. Below 10% crosstalk was one of the design specifications of our DM system. The total required force is about 16 μN after adding actuators beneath the center pillar. Referring to Figure 6, we see that a 1 N/m actuator has a width of 40 μm.

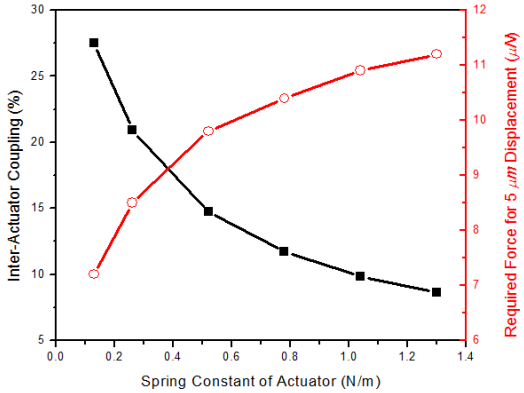

Figure 7. Inter-actuator coupling (crosstalk) and membrane deformation.

The resonant frequency of the DM system is simulated with the center cantilever actuator (1000 μm length x 10 μm thickness x 40 μm width having 1 N/m spring constant) added to STEP 3 as a boundary condition. Figure 8 shows the first two resonance modes and corresponding frequency. The over 1 KHz frequency in the DM system specification for large diameter telescopes is easily satisfied with this DM system. Overall, the mass and spring constant define the resonant frequency of the DM system (see equation 3). Therefore, the actual resonant frequency can be slightly lower than the simulation result due to additional mass on the actuators.

$$\mathrm{f} = \frac{1}{2\pi}\sqrt{\frac{k}{m}} \qquad (3)$$

where f is resonance frequency, k is the spring constant, and m is mass of entire resonator.

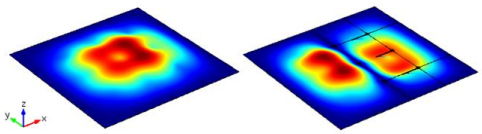

Membrane Coating Material	Resonant Frequency (*KHz*)	
	1st mode	2nd mode
Al	1.409	1.665

Figure 8. Initial resonance modes and corresponding frequency of DM system.

Materials in a MEMS device should work in elastic range (under Yield strength or tensile strength) to avoid device damage and/or non-linear behavior. Tensile strength of evaporated *Al*

and spin coated SU-8 are 151 MPa [11] and 60 MPa [12] respectively. Simulation for the maximum stress of the DM system is done using the boundary conditions of STEP 1. The maximum stress with 10 µm maximum stroke is 17.26 MPa, which is ~ 3 times lower than the tensile strength of SU-8. Therefore, this DM design will possess a good safety factor.

3.2. Horseshoe Shaped Lorentz Actuator

Actuator deflection and Joule heating are studied in this section. Various spring cantilever geometries were considered as supports for the crossbar. They included a thin film copper metal forming cantilever supports, and thicker copper metal formed using an electroplating process.

Various thickness and widths of 300 µm long copper cantilevers were considered as soft structures that can be deformed by an applied load on the thick crossbar. Figure 9 shows calculation results for various cantilevers. We can see that the desired spring constant of the actuator (1 N/m) can be achieved with a copper cantilever 1 µm thick, 80 µm wide, and 300 µm long. The crossbar thickness required for rigidity during actuation is calculated using equation 2. It is found that a 25 µm thick crossbar deforms about 0.18 µm with the applied load of 16 µN on the crossbar at the center pillar location. 25 µm was selected as an appropriate crossbar thickness. This thickness will require an electroplating process for fabrication.

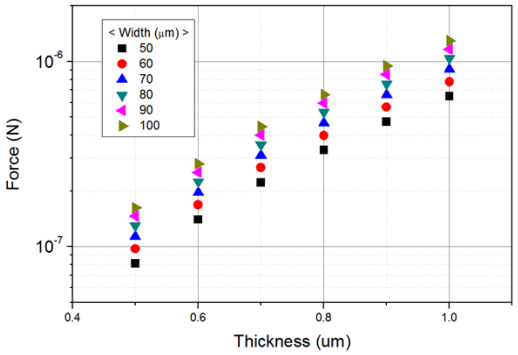

Figure 9. Spring constant with various thickness and width of the single loop serpentine (left) and double loops serpentine (right).

Joule heating can be a significant problem for Lorentz devices due to the higher current flow in the structures compared to electrostatic actuators. This heat could seriously affect the membrane deformation motion by thermal stress, as well as convection of airflow surrounding the membrane. The simulation results for Joule heating are shown in Figure 10. These simulations were done for a 2080 µm long x 200 µm wide x 25 µm thick copper crossbar, supported by 300 µm long cantilevers of various widths and thicknesses.

For the desired 5 µm motion, to 16 µN force is needed. This force corresponds to a 7.7 mA current flowing in the crossbar, paired with a 1 Tesla magnet below the actuators. Referring to Figure 10, we can see that the temperature variation (ΔT) is less than 0.1 K. This temperature change is very small, and so thermally induced mechanical stress does not need to be considered for our design.

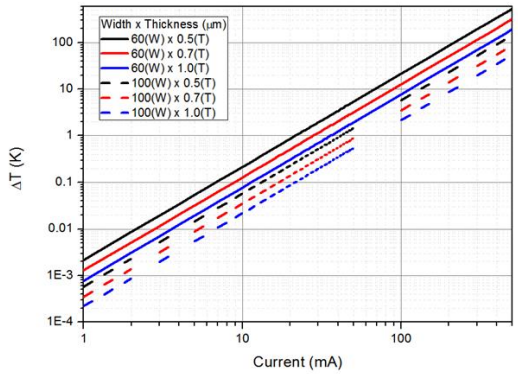

Figure 10. Maximum temperature change on the center of crossbar vs. current level of various thicknesses and widths of two horseshoe shaped Lorentz actuators.

4. Conclusions

The design and analysis of a MEMS based LCL-DM with a soft polymer based mirror membrane is presented. The mechanical crosstalk of actuators on the membrane was successfully simulated. The crosstalk was shown to vary from 10 to 25 % depend on actuator softness. In addition, the thermal stress induced by Joule heating is determined to be minimal for the required low operation current of the LCL-DM. The designed LCL-DM offers low voltage operation compared to conventional electrostatic DMs.

5. References

1. Madec, P. -Y. (2012). Overview of deformable mirror technologies for adaptive optics and astronomy. In *SPIE Astronomical Telescopes+ Instrumentation* (pp. 844705–844705). International Society for Optics and Photonics. http://proceedings.spiedigitallibrary.org/proceeding.aspx?articleid=1358867
2. Vera-Díaz, F. A., and Doble, N. (2012). *The Human Eye and Adaptive Optics*. INTECH Open Access Publisher. http://cdn.intechopen.com/pdfs-wm/26714.pdf
3. Vinevich, B. S., Evdokimovich, L. N., Safronov, A. G., and Smirnov, S. N. (2004). Application of deformable mirrors in industrial CO2 lasers. *Quantum Electronics*, ***34***(4), 333. http://doi.org/10.1070/QE2004v034n04ABEH002677
4. Bell, D. J., Lu, T. J., Fleck, N. A., and Spearing, S. M. (2005). MEMS actuators and sensors: observations on their performance and selection for purpose. *Journal of Micromechanics and Microengineering*, ***15***(7), S153–S164. http://doi.org/10.1088/0960-1317/15/7/022
5. Yellin, M. (1976). Using Membrane Mirrors In Adaptive Optics (**Vol. 0075**, pp. 97–102). http://doi.org/10.1117/12.954743
6. Hsu, T. -R. (2008). *MEMS & Microsystems: Design, Manufacture, and Nanoscale Engineering*. John Wiley & Sons.
7. Lv, X., Wei, W., Mao, X., Chen, Y., Yang, J., and Yang, F. (2015). A novel MEMS electromagnetic actuator with large displacement. *Sensors and Actuators A: Physical*, ***221***, 22–28. http://doi.org/10.1016/j.sna.2014.10.028
8. Ulaby, F. T. (2005). *Electromagnetics for Engineers*. Pearson/Prentice Hall.
9. J. M. Shaw, J. D. G. (1997). Negative photoresists for optical lithography. *IBM Journal of Research and Development*, (1.2), 81 – 94. http://doi.org/10.1147/rd.411.0081
10. Friese, C., and Zappe, H. (2008). Deformable Polymer Adaptive Optical Mirrors. *Journal of Microelectromechanical Systems*, ***17***(1), 11–19. http://doi.org/10.1109/JMEMS.2007.913075
11. Read, D. T., McColskey, J. D., Geiss, R., and Cheng, Y.-W. (2003). Microtensile Testing of Thin Films in the Optical and Scanning Electron Microscopes. In *AIP Conference Proceedings* (**Vol. 683**, pp. 353–356). AIP Publishing. http://doi.org/10.1063/1.1622495
12. MICROCHEM. (2007). SU-87 2000 Specification. http://christophe.yamahata.fr/projects/pdf/51.pdf

6. Acknowledgements

This work was undertaken with the support of the National Research Council (NRC) Herzberg, Victoria, Canada and University of Manitoba Graduate Fellowship (UMGF).

7. Appendix

Appendix 1. Material properties for modelling and COMSOL simulation

Properties / Material	SU-8 2025	Al	Cu	<100 > c-Si
Density (Kg/m^3)	1219	2700	8960	2329
Young's Modulus (GPa)	2	70	130	162
Poisson's Ratio	0.22	0.35	0.34	0.28
Electrical Conductivity (S/m)	N.A.	3.54×10^7	3.33×10^7	1.56×10^{-3}
Relative permittivity	1	1	1	11.7
Thermal Conductivity (W/mK)	0.3	237	401	130
Heat Capacity at Constant Pressure (J/K)	1420	904	384	700
Coefficient of Thermal Expansion (m/K)	5.2×10^{-5}	2.31×10^{-5}	1.65×10^{-5}	2.6×10^{-6}
Specific Heat (J/Kg/K)	-	898.7	385	-